

# Fractional topological phases and broken time reversal symmetry in strained graphene

Pouyan Ghaemi,<sup>1,2,3</sup> Jérôme Cayssol,<sup>1,4,5</sup> D. N. Sheng,<sup>6</sup> and Ashvin Vishwanath<sup>1,2</sup>

<sup>1</sup>*Department of Physics, University of California at Berkeley, Berkeley, CA 94720, USA*

<sup>2</sup>*Materials Sciences Division, Lawrence Berkeley National Laboratory, Berkeley, CA 94720*

<sup>3</sup>*Department of Physics, University of Illinois, Urbana, IL 61801*

<sup>4</sup>*LOMA (UMR-5798), CNRS and University Bordeaux 1, F-33045 Talence, France*

<sup>5</sup>*Max-Planck-Institut für Physik Komplexer Systeme, Nöthnitzer Str. 38, 01187 Dresden, Germany*

<sup>6</sup>*Department of Physics and Astronomy, California State University, Northridge, California 91330, USA*

Recently several lattice models with topologically nontrivial flat bands have been shown to host phases such as fractional Chern insulators<sup>1-8</sup> and fractional topological insulators<sup>9-11</sup>. Despite wide interest, an experimentally viable system with these exotic topological orders is still lacking. On the other hand a recent experiment<sup>12</sup> has confirmed that strain can be used to control the electronic states of graphene and create flat pseudo-Landau levels in the absence of external magnetic field<sup>13,14</sup>. These pseudomagnetic fields respect time reversal symmetry and far exceed the strongest magnetic fields available. Here we show that graphene under strain is a natural playground in the search for exotic many-body phases, such as fractional topological insulators and flat band superconductors, in addition to fractional Hall states. At fractional filling, Coulomb interactions stabilize a valley polarized Laughlin liquid that spontaneously breaks time reversal symmetry. On tuning the short ranged interactions, a valley unpolarized fractional phase emerges, which is a time reversal symmetric analog of the Laughlin liquid. Further tuning interactions leads to a spin triplet superconductor. On raising the filling to the neutrality point, we find either a ferromagnet or a valley polarized state, depending on the strength of on-site interactions. The importance of interaction engineering to realize these phases introduces directions for future experimental research to tune interactions in strained graphene as well as in other potential platforms such as patterned electron gases<sup>15</sup> and cold atoms in hexagonal lattices<sup>16</sup>.

PACS numbers:

## I. INTRODUCTION

The single atomic layer of carbon atoms in graphene can be strained and the resulting deformation modifies hopping amplitudes of electrons between carbon sites, thereby producing a pseudo-magnetic field with opposite sign for the valleys  $\mathbf{K}_{\pm}$ <sup>17</sup>. For some particular strain patterns, the generated pseudo-magnetic field can be made uniform yielding a pseudo-Landau level (PLL) structure at zero magnetic field<sup>13</sup>. Such strain induced PLLs have been reported experimentally with effective pseudo-magnetic fields as large as 300 T<sup>12</sup>. This unique system provides electronic flat bands while still preserving the time reversal  $\mathcal{T}$  symmetry. It is therefore a very natural candidate to realize a time reversal symmetric version of the fractional Quantum Hall (FQH) phase, called fractional topological insulators<sup>9-11</sup>, and also superconducting phases. The latter are suppressed by real magnetic fields, but are more natural here, and are expected to benefit from the flat band dispersion<sup>18-20</sup>. Moreover the longstanding issue of valley and spin ferromagnetism in graphene which is still under debate<sup>21-25</sup> must be reexamined in this time-reversal invariant flat band system which is naturally very susceptible to develop various orders.

Here, we address the physics of graphene under strong pseudo-magnetic field in presence of long range Coulomb and short range Hubbard interactions, using mean field and numerical exact-diagonalization techniques. We show how tuning these interactions, for neutral graphene

can stabilize phases with valley or spin polarization, and for fractionally filled graphene lead to fractional valley Hall insulator, a fractional topological insulator where valley plays the role of spin, and spin triplet superconducting phases. In addition, valley polarized FQH states, that spontaneously break  $\mathcal{T}$  symmetry naturally emerge. Conceivably, these may be realized with large energy gaps, given the strong pseudofields that can be generated by mechanical strain.

## II. FLAT BANDS OF STRAINED GRAPHENE

The tight-binding Hamiltonian of non-interacting strained graphene reads

$$H = \sum_{\mathbf{r}_i} \sum_{a=1,2,3} (t + \delta t_a(\mathbf{r}_i))(a^\dagger(\mathbf{r}_i)b(\mathbf{r}_i + \boldsymbol{\delta}_i) + h.c.) \quad (1)$$

where  $\delta t_a(\mathbf{r}_i)$  is the strain-induced variation of the nearest neighbor hopping amplitude (with respect to the unperturbed value  $t \simeq 2.7$  eV) between A-site at  $\mathbf{r}_i$  and B-site at  $\mathbf{r}_i + \boldsymbol{\delta}_i$  of the bipartite honeycomb lattice<sup>17</sup>. The vectors  $\boldsymbol{\delta}_a$  connect any A-carbon atom to its three B-type nearest neighbours. In the absence of strain ( $\delta t_a = 0$ ), the lattice Hamiltonian can be easily diagonalized and the low energy excitations correspond to linearly dispersing states close to the two Dirac points at momenta  $\xi \mathbf{K}$  with  $\mathbf{K} = (4\pi/3\sqrt{3}a)\mathbf{e}_x$  and  $\xi = \pm 1$ .

If the lattice deformation is smooth there is no large momentum scattering and the valleys remain decou-

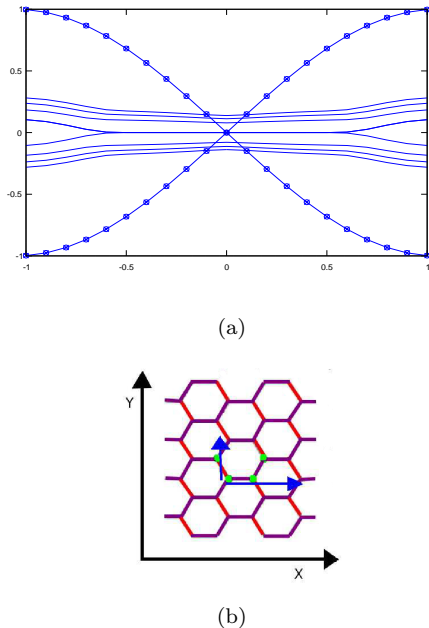


FIG. 1: (a) Dispersion of low energy states close to one of Dirac points as a function of  $k$  for unstrained (dotted lines) and strained (solid lines) graphene. In order to generate a uniform field in the Landau gauge, we assume a simple  $\delta t_{ij}$  pattern (b) where the hopping amplitude only changes on one type of bonds (red bonds in (b)) and varies along  $y$  direction as  $\delta t = \Delta y$ . With this choice of  $\delta t_{ij}$ , the potential vector is given by  $A_x = -B_e y$  and  $A_y = 0$ , thereby yielding a uniform pseudo magnetic field. For a magnetic flux  $\Phi$  in units of magnetic flux quantum  $\Phi_0$  through the hexagon unit cell, the change in the hopping parameter per lattice spacing is  $\Delta t \sim t\Phi$  where  $t$  is non-perturbed hopping amplitude<sup>26</sup>. So  $\frac{\Delta t}{t} \sim \frac{B_e}{\Phi_0} a^2$  where  $a$  is the lattice spacing. The maximum possible length of the sample then would be  $a \frac{t}{\Delta t} \sim \frac{\Phi_0}{a B_e} \sim 100 \text{ nm}$ .

pled. At low energy, the lattice problem reduces to Dirac fermions with 2 flavors, valley and spin, immersed in a valley dependent vector potential  $\mathbf{A}_\xi(\mathbf{r}) = \xi \sum_{a=1,2,3} \delta t_a(\mathbf{r}) e^{i\mathbf{K} \cdot \boldsymbol{\delta}_a}$  which is minimally coupled to the momentum of excitations relative to Dirac point  $\xi$ . In contrast to the full  $SU(4)$  symmetry of graphene in an external real magnetic field<sup>21</sup>, the internal symmetry of strained graphene is  $SU(2)$  for the spin and only  $Z_2$  for the valley degree of freedom. In spite of those differences, the pseudo-magnetic field also provides a Landau level like structure  $E_n = \xi \sqrt{2e\hbar v_F^2 B} |n|$ , where  $n$  is the relative integer labelling the Landau levels. See Fig. 1 for the band structure of graphene with a particular choice of deformation.

### III. INTERACTION MODELS IN THE ZERO ENERGY FLAT BAND.

In this work, we focus on interaction effects within the four-fold degenerated zero-energy flat band ( $n = 0$ ). As for an ordinary magnetic field, the Coulomb interaction  $V(\mathbf{r}_i - \mathbf{r}_j) n(\mathbf{r}_i) n(\mathbf{r}_j) = e^2 n(\mathbf{r}_i) n(\mathbf{r}_j) / 4\pi\epsilon |\mathbf{r}_i - \mathbf{r}_j|$  is likely the dominant interaction due to the poor screening in neutral graphene. Here the density  $n(\mathbf{r}) = \sum_{\xi, \xi' = \pm} e^{i(\xi\mathbf{K} - \xi'\mathbf{K}) \cdot \mathbf{r}} n_{\xi\xi'}(\mathbf{r})$  includes contributions from low energy (long wavelength) excitations near both valleys. Those excitations are created by the field operators  $\psi_\xi^\dagger(\mathbf{r})$  for valley  $\xi$ , and  $n_{\xi\xi'}(\mathbf{r}) = \psi_\xi^\dagger(\mathbf{r}) \psi_{\xi'}(\mathbf{r})$ . Nevertheless recent first-principles calculations point towards sizable nonlocal Hubbard correlations as well<sup>27</sup>. In this work we explore the phase diagram of strained graphene for arbitrary values of Hubbard correlations (both positive and negative). We only consider the on-site Hubbard interaction  $U_0 \delta_{ij} n(\mathbf{r}_i) n(\mathbf{r}_j)$  and the next-nearest neighbour (NNN) coupling  $U_{nnn}$ . The nearest neighbour interaction is not effective in presence of strong pseudo-magnetic field because the noninteracting wave functions are localized on one sublattice in the zero energy PLL.

### IV. SPONTANEOUSLY BROKEN SYMMETRY PHASES AT HALF-FILLING

Band structure of neutral graphene (filling factor  $\nu = 0$ ) under triaxial strain<sup>12-14</sup> corresponds to the half-filled zero energy flat band, i.e. two electrons per Landau orbital. There is a natural competition between a valley ferromagnet  $\Psi_V = \prod_k c_{R,k,\uparrow}^\dagger c_{R,k,\downarrow}^\dagger |0\rangle$  and spin ferromagnet  $\Psi_S = \prod_k c_{R,k,\uparrow}^\dagger c_{L,k,\uparrow}^\dagger |0\rangle$  states where  $k$  labels different Landau orbitals in  $n = 0$  PLL. We first consider the case of pure Coulomb interaction ( $U_0 = U_{nnn} = 0$ ):

$$V(\mathbf{r} - \mathbf{r}') n(\mathbf{r}) n(\mathbf{r}') = \frac{e^2}{4\pi\epsilon |\mathbf{r} - \mathbf{r}'|} \sum_{\xi, \xi' = \pm} \sum_{\eta, \eta' = \pm} e^{i[(\mathbf{K}_\xi - \mathbf{K}_{\xi'}) \cdot \mathbf{r} - (\mathbf{K}_\eta - \mathbf{K}_{\eta'}) \cdot \mathbf{r}']} n_{\xi\xi'}(\mathbf{r}) n_{\eta\eta'}(\mathbf{r}'). \quad (2)$$

Using Hartree-Fock method<sup>21,22</sup> we calculate the interaction energy in valley and spin polarized states. The dominant terms in interaction (2) correspond to  $n_{++}(\mathbf{r}) n_{++}(\mathbf{r}'), n_{--}(\mathbf{r}) n_{--}(\mathbf{r}')$ ,  $n_{++}(\mathbf{r}) n_{--}(\mathbf{r}')$  and  $n_{--}(\mathbf{r}) n_{++}(\mathbf{r}')$  interactions and give the same energy for valley or spin polarized states. We find that the intervalley scatterings  $n_{+-}(\mathbf{r}) n_{-+}(\mathbf{r}')$  and  $n_{-+}(\mathbf{r}) n_{+-}(\mathbf{r}')$  lift this degeneracy by favoring the valley polarization. Note that for real magnetic field, those so-called backscattering terms are absent in the  $n = 0$  LL due to the symmetry of the eigenspinors. Nevertheless other sub-dominant lattice effects (electrostatic ones) were then found to stabilize the valley ferromagnet as well<sup>21,22</sup>. Also contrary to the real magnetic field Hall effect, long range Coulomb interaction prefers an Ising-like  $Z_2$  valley polarized state

rather than a more general  $SU(2)$ -valley-rotated state (see Supplementary).

We now introduce short ranged Hubbard correlations and compute numerically the total energy of finite size systems on a torus. First we have checked that the valley polarized state has indeed lower energy for the pure Coulomb case (Fig. 2). As a simplest type of perturbation, we have introduced strictly *on-site Hubbard interaction*  $U_0\delta_{ij}n(\mathbf{r}_i)n(\mathbf{r}_j)$  on top of the bare Coulomb interaction. As expected solely the energy of the valley polarized state is modified while the spin polarized state is unchanged (Fig. 2). Indeed in the valley polarized state, double occupancy of a single site is allowed thereby providing an energy proportional to  $U_0$ . In contrast, in the spin polarized state, double occupancy is forbidden by the Pauli principle and the total energy is therefore insensitive to the on-site Hubbard coupling. As a result, the competing valley polarized state (empty square, Fig. 3) is the groundstate as long as the Hubbard interaction is not too repulsive ( $U_0 < 0.5$  in units of  $e^2/4\pi\epsilon a \simeq 10$  eV), including the pure Coulomb case and further increase of the on-site Hubbard interaction stabilize the spin ferromagnet state.

In order to test the sensitivity of the phase diagram with respect to the details of the short range part of the interaction, we have replaced the on-site Hubbard interaction by the *NNN coupling*  $U_{nnn}$ . Interestingly we have obtained the reverse phenomenology where repulsive  $U_{nnn}$  tends to valley polarize the system. Indeed both spin and valley ferromagnets are affected by the Hubbard NNN coupling, and the spin polarized state (filled triangle) is now stabilized for sufficiently attractive ( $U_{nnn} < -0.5$  in units of  $e^2/4\pi\epsilon a \simeq 10$  eV). The electrons in the opposite valleys are easier to pair up driven by the NNN attracting interaction. These results can also be derived within the Hartree-Fock approximation (see supplementary).

The very contrasted phase diagrams for strictly one-site and NNN couplings thus demonstrate that the ground state is very sensitive to lattice scale details of the interaction (Fig. 2,b). This is related to the fact that competing states are nearly degenerated if one only takes into account the long distance Coulomb interaction. Unfortunately the actual values of  $U_0$  and  $U_{nnn}$  in strained graphene samples are not known so it is difficult to conclude reliably whether spin or valley gets polarized. Nevertheless recent first principles calculations yield total on-site coupling  $U_0 = 9.3$  eV and total NNN coupling of 5.4 eV for freestanding (and unstrained) graphene in zero magnetic field<sup>27</sup>. In our units ( $e^2/4\pi\epsilon a \simeq 10$  eV) those values correspond to  $U_0 \simeq 1$  pointing towards the spin ferromagnetic phase (Fig. 2,b). The deviation  $U_{nnn} \simeq -0.04$  of the NNN coupling from its bare Coulomb value can be neglected. Using gating or different substrates, it could be possible to switch the ground-state between spin ferromagnet and valley Ising ferromagnet. Spin polarized STM and Kerr imaging could indeed detect these competing ground states. Note, the

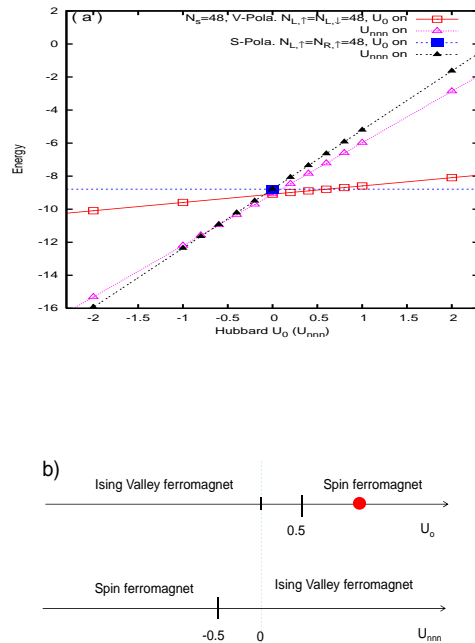


FIG. 2: (Color online) Filling  $\nu = 0$ . (a) The energy of the different Hartree-Fock states are compared in the presence of either on-site Hubbard term ( $U_0$ ) or NNN one ( $U_{nnn}$ ). All energies remain linearly depending on Hubbard  $U_0$  ( $U_{nnn}$ ) for all parameters. The degeneracy of LL orbits is  $N_s = 48$  while electron number in different valleys (or spins) sum up to  $N_e = 96$ . The lattice we considered has  $96 \times 96$  sites. (b) Phase diagrams for two different types of Hubbard correlations: one-site ( $U_0$ ) and NNN ( $U_{nnn}$ ). The energy is in units of  $e^2/4\pi\epsilon a$  with  $a$  as the distance between the NN sites. Red dots indicate the values of the coupling strengths for freestanding and unstrained graphene according to Ref.<sup>27</sup>.

valley Ising ferromagnet is an integer quantum Hall state with two units of quantized Hall conductance, that spontaneously breaks time reversal symmetry.

## V. FRACTIONALIZED PHASES AND SUPERCONDUCTIVITY

Fractional Hall states in graphene under an external magnetic field were reported experimentally only very recently<sup>28–30</sup>. Although strain produces flat pseudo Landau levels, it is not evident that interactions can generate incompressible phases at fractional filling in time-reversal invariant strained graphene. Using exact diagonalization of finite size systems, we actually find such interaction-driven ordered states at filling  $\nu = -2 + 2/3 = -4/3$  (i.e. at this filling the electron density can fill  $2/3$  of a single Landau level, of the four sets of degenerate Landau levels). At this particular filling, a natural question to ask is whether: i) a single valley develops a full  $2/3$  Laughlin state thereby *breaking time-reversal symmetry*, or ii) each valley builds up its own  $1/3$  Laughlin state

in a *time-reversal invariant* way, for the orbital wavefunction. Below it is shown that both these scenarios are possible leading to qualitatively different states than the  $2/3$  FQH states under real magnetic field studied so far in graphene sheets<sup>31,32</sup> and in GaAs Hall bilayers<sup>33</sup>. For graphene with dominant Coulomb interaction, the  $2/3$  valley polarized state is realized, with spins in a singlet. In order to destabilize this  $2/3$  state, we have introduced a form of NNN interaction in addition to Coulomb interactions. For convenience we assume this acts only between opposite valley fermions ( $U_{nnn}^{op}$ ), while electrons in the same valley only interact via Coulomb potential Eq. 2 (i.e.  $U_{nnn}^s = 0$ ). Then a valley unpolarized Hall state with nine fold degenerated groundstate is realized for intermediate coupling ( $-0.73 < U_{nnn}^{op} < -0.58$ ), which is labeled a fractional topological insulator (FTI). Moreover a spin triplet superconducting state is stabilized at larger attraction (Fig. 3). Hereafter we present detailed numerical results supporting the existence of each of those quantum phases.

### A. Laughlin $2/3$ state in a single valley

For the pure Coulomb interaction ( $U_{nnn} = 0$ ), corresponding to realistic graphene, the ground state is valley polarized, thereby spontaneously breaking the time-reversal invariance of the strained graphene Hamiltonian. Spins are in a singlet state<sup>33</sup>, as in the spin singlet  $2/3$  FQHE state<sup>33</sup>. The observation of such a state can be made easier by the very large values of pseudomagnetic field seen in a single valley.

### B. Time-reversal invariant state

In the range of interaction strength ( $-0.73 < U_{nnn}^{op} < -0.58$ ), an interesting quantum phase emerges with a nine-fold near degenerating states forming the ground state manifold (GSM) as demonstrated in Fig. 3. The momentum quantum numbers of these states are at  $k = 0$  and other  $k$  determined by shifting the momentum of each electron by an integer multiple of  $2\pi/N_s$ , where  $N_s$  is the PLL orbital degeneracy. This determines three different momenta sectors ( $k = 0, \pi/3$ , and  $2\pi/3$ ) and there are three near degenerate states in each sector. These sectors can be considered as ground state flows from one sector to another upon inserting flux through adding the twist boundary phase. In this parameter region, we see that other excited states (Fig 3a, lines without symbols) are well separated from the lower energy the GSM (Fig. 3a, lines with symbols). By tuning the boundary phase for a system at  $U_{nnn}^{op} = -0.6$ , we see that the nine near degenerate states remain well separated from other excited states as shown in Fig. 3b.

As a second evidence, we further perform valley-pseudospin Chern number calculation<sup>34,35</sup> by adding the same boundary phase along x-direction, and the opposite

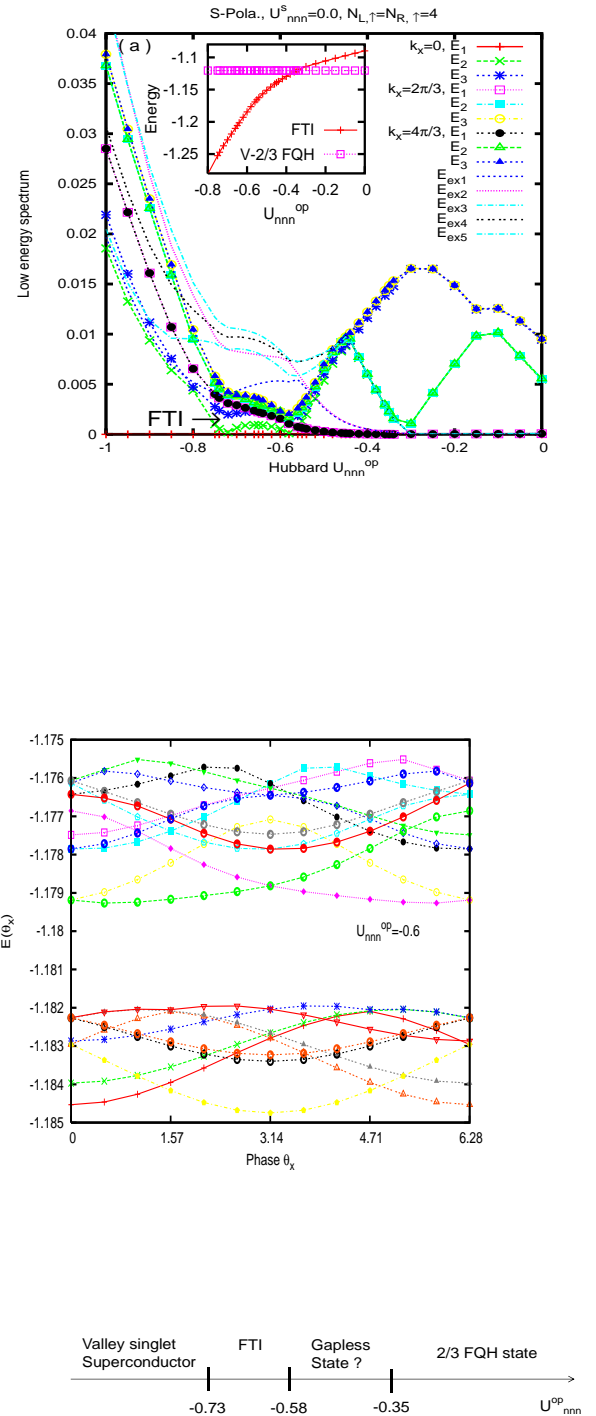


FIG. 3: (Color online) (a) Fractional topological insulating (FTI) phase at filling  $\nu = -2 + 2/3$  ( $\nu = 0$  is the neutral point). The noninteracting orbitals are determined on a  $24 \times 24$  lattice with a pseudomagnetic flux  $\Phi_0/48$  per hexagon. Then the effective interaction is calculated in the  $n = 0$  PLL whose degeneracy is  $N_s = 12$  per spin direction and per valley. The low energy spectrum is calculated for  $N_e = 8$  ( $N_L = N_R = 4$ ) electrons with polarized spin occupying those  $N_s = 12$  states. In the parameter region  $-0.73 < U_{opp} < -0.58$ , the nine lowest energy states become close together and almost degenerated, thereby forming the groundstate manifold (GSM). (b) The boundary phase dependence and the robust gap between the GSM and other excited states are shown for  $U_{nnn}^{op} = -0.6$  inside the FTI (fractional topological insulator) phase. (c) A phase diagram as a function of  $U_{nnn}^{op}$  for spinless electrons. Energies are given in units of  $e^2/4\pi\epsilon a \simeq 10$  eV.

ones along y-direction for both valleys<sup>36,37</sup>. This generalized pseudospin Chern number is well defined as the electron number in each valley is conserved thus that the valley-pseudospin is a good quantum number. We find a total Chern number quantized to 6 for all nine levels, characterizing the 2/3 fractionalized valley spin-Hall effect. This spin polarized state turns out to have lower energy comparing to the valley polarized 2/3 FQHE Laughlin state as shown in the inset of Fig. 3. In order to realize the FTI, one needs to be able to tune an attraction between electrons in the opposite valleys. this is further discussed below, here we simply note that Coulomb interactions alone tend to polarize valleys, a form of flat band ferromagnetism, but this is not a necessary outcome of other repulsive interactions.

Further evidence of such an FTI state (here since valley plays the role of spin it may also be called the fractional valley Hall insulator) can be obtained by turning on and increasing the intravalley part of the NNN coupling  $U_{nnn}^s$  and compare the current state with the valley-decoupled  $1/3 + 1/3$  fractional valley Hall insulator at large  $U_{nnn}^s$  limit. Indeed, we find there is no phase transition between this state and the decoupled fractional valley Hall insulator, see in the supplementary.

### C. Triplet superconducting state

Consider tuning  $U_{nnn}$  without distinguishing the valleys. For sufficiently large attraction (Fig. 4), the ground state of the spinful model becomes spin-polarized at  $U_{nnn} \leq -0.8$ . (Note, when added to the Coulomb repulsion, this ends up giving a somewhat smaller but still attractive next nearest neighbor interaction of  $U_{nnn}^{\text{tot}} = -0.2$ ). We have identified this phase as a spin triplet and valley singlet superconducting state with a small but finite superfluid density  $n_s$ . We obtain  $n_s$  from the change of the ground state energy  $E_g$  with adding a small phase twist  $\theta$  as  $n_s = 1/2 \frac{\partial^2 E_g}{\partial \theta^2}$ <sup>36,38</sup>. Moreover the finite jump for  $n_s$  at the transition point  $U_{nnn} = -0.8$  (inset of Fig. 4) indicates the first-order transition between the valley polarized state and the spin polarized superconducting state. The typical momentum dependence of energy is quite opposite to the 2/3 FQHE case as the ground state is in the  $k = 0$ -sector without quasi-degeneracy (Fig. 4c). Indeed using the extended BCS framework with next-nearest neighbour interaction, it can be shown that the spin triplet superconducting state has generically lower energy than the spin singlet, since more inter-valley scatterings are participating in the pairing (see supplementary). Such flat band superconductivity is expected to have enhanced pairing<sup>18-20</sup>, arising from the larger density of states (see Supplementary).

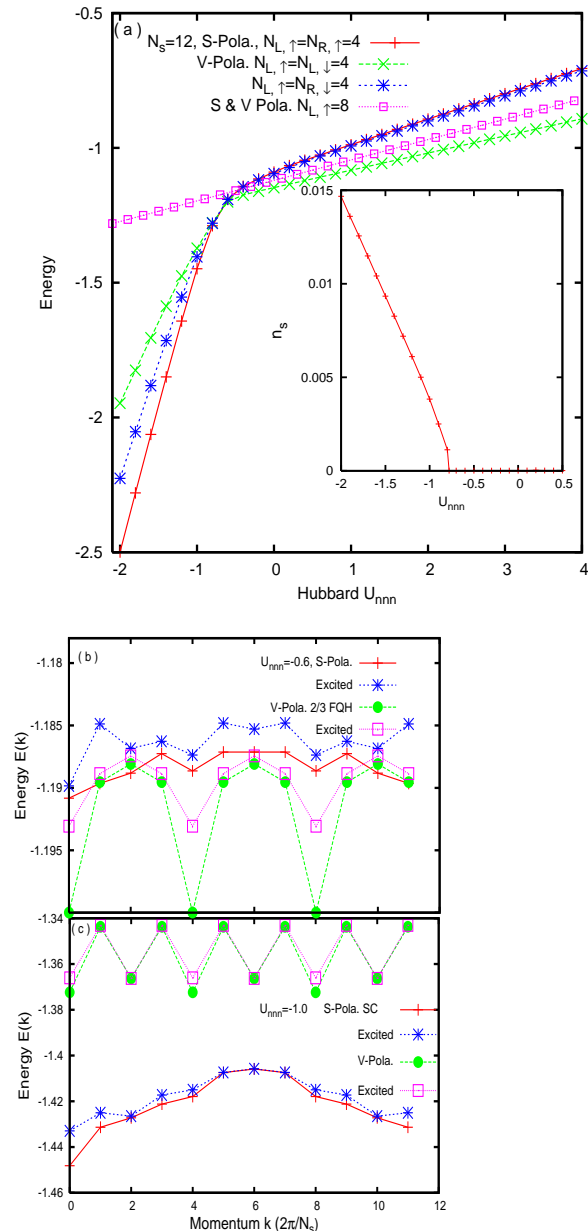


FIG. 4: (Color online) (a) The energy of different states at filling  $\nu = -2 + 2/3$  as a function of  $U_{nnn}$ . The LL degeneracy is  $N_s = 12$  and we have  $N_e = 8$  electrons. The lattice system has  $24 * 24$  sites. With weak attraction or repulsion ( $U_{nnn} > -0.8$ ), the ground state is valley polarized FQHE state. At  $U_{nnn} < -0.8$  side, the valley unpolarized superconducting state with the spontaneous spin-polarization wins. This superconducting phase is characterized by a finite superfluid density as shown in the inset. (b-c) Two lowest energies in each momentum sector for spin polarized and valley polarized states are shown as a function of  $k$  at  $U_{nnn} = -0.6$  (b) and  $-1.0$  (c). Energies are given in units of  $e^2/4\pi\epsilon a \simeq 10$  eV.

## VI. CONCLUSIONS

We have shown that strained graphene hosts various fractional topological phases which depend on the detailed structure of the electron-electron interactions. For larger attractive interactions, spin triplet superconductivity may also be realized. The most readily realized are Laughlin states that spontaneously break time reversal symmetry by selecting a valley. These occur with the unmodified Coulomb interactions. Potentially, these states may be realized with elevated energy scales, allowing for the stabilization of fragile states. As an estimate the  $\nu = 1/3$  energy gaps range from the theoretical value of  $\delta_{\frac{1}{3}} \sim 0.1E_C$  to observed experimental values which are typically smaller  $\delta_{\frac{1}{3}} \sim 0.01E_C$ , with  $E_C \sim 7 \times 10^2$  Kelvin.  $\sqrt{B(\text{Tesla})}$ , for a suspended sample. For the observed 300 Tesla pseudofield<sup>12</sup>, the gap estimate would then range from  $10^3$  to  $10^2$  Kelvin. In current experiments, the nano-scale strained regions admitting just a few Landau level states, and are strongly coupled to a metallic substrate outside. Future experiments on insulating substrates could address bigger strained regions. Nevertheless, signatures of fractional states in restricted domains and interactions with itinerant electrons outside the strained region will be important topics for future study. The  $n = 0$  Landau levels are expected to be the best isolated, since they occur at the Dirac point, where the density of itinerant states is the smallest.

We discussed how the valley unpolarized phase, with time reversed Laughlin states occupying opposite valleys, could be stabilized. This is related to the so called fractional topological insulators, where valley plays the role of spin. However, since these differ in their transformation under time reversal, edge states are not protected in this phase. However, the topological order and fractional excitations in the bulk are robust characteristics of the phase. This state emerged on altering the short ranged interactions between electrons in the same and opposite valleys. Interesting proposals for altering short ranged interactions using substrates with momentum dependent dielectric susceptibility has been discussed<sup>39</sup>. The most realistic form of interactions required to stabilize the fractional valley Hall insulator is however left for future work.

Finally, we discussed superconductivity, which emerged in part of the phase diagram. The physical properties of such superconductors that arise from unusual flat band normal states requires further work. In addition to strained graphene, other promising experimental realizations include patterned electron gases<sup>15,40</sup> and cold atoms in hexagonal optical lattices<sup>16</sup>. The latter may be particularly relevant for studying the attractive interaction regime. This study opens the prospect of discovering a series of new nontrivial topological phases at other fractional fillings and in higher pseudo Landau levels as well.

## Acknowledgments

We would like to thank J. Alicea and N. Regnault for useful comments. JC acknowledge support from EU/FP7 under contract TEMSSOC and from ANR through project 2010-BLANC-041902 (ISOTOP). This work is also supported by DOE Office of Basic Energy Sciences under grant DE-FG02-06ER46305 (DNS).

### Appendix A: Supplementary materials

#### 1. Noninteracting strained graphene

Here we consider noninteracting spinless fermions on the honeycomb lattice (including of spin is straightforward). The triangular Bravais lattice  $\mathbf{r}_{mn} = m\mathbf{a}_1 + n\mathbf{a}_2$  is generated by the basis vectors:

$$\mathbf{a}_1 = \sqrt{3}a\mathbf{e}_x \text{ and } \mathbf{a}_2 = \frac{\sqrt{3}a}{2}(\mathbf{e}_x + \sqrt{3}\mathbf{e}_y), \quad (\text{A1})$$

and the vectors:

$$\boldsymbol{\delta}_1 = \frac{a}{2}(\sqrt{3}\mathbf{e}_x + \mathbf{e}_y), \boldsymbol{\delta}_2 = \frac{a}{2}(-\sqrt{3}\mathbf{e}_x + \mathbf{e}_y), \boldsymbol{\delta}_3 = -a\mathbf{e}_y, \quad (\text{A2})$$

connect any A atom to its three nearest B atoms,  $a = 0.142$  nm being the length of the carbon-carbon bond. The area of the unit cell is  $\mathcal{A}_c = 3\sqrt{3}a^2/2$ .

#### 2. Strained induced gauge potential

In the absence of interactions, the tight-binding Hamiltonian of strained graphene (Eq. 1 in the main text) can be written as:

$$H_0 = \sum_{\mathbf{r}_{mn}} \sum_{i=1,2,3} (t + \delta t_i(\mathbf{r}_{mn})) (a^\dagger(\mathbf{r}_{mn})b(\mathbf{r}_{mn} + \boldsymbol{\delta}_i) + h.c.), \quad (\text{A3})$$

where second quantization operators  $a(\mathbf{r}_{mn})$  and  $b(\mathbf{r}_{mn} + \boldsymbol{\delta}_i)$  annihilate a fermion at A-type and B-type sites respectively. The strain is described by the deformation field  $\delta t_i(\mathbf{r}_{mn})$  of the nearest-neighbour hopping element between sites  $\mathbf{r}_{mn}$  and  $\mathbf{r}_{mn} + \boldsymbol{\delta}_i$  with respect to the unperturbed value  $t$ . Note that the deviations  $\delta t_i(\mathbf{r}_{mn})$  are real quantities and must be smaller than  $t$ .

In the absence of strain ( $\delta t_i(\mathbf{r}_{mn}) = 0$ ), the lattice Hamiltonian can be easily diagonalized and the low energy excitations correspond to the states close to the two gapless Dirac points  $\mathbf{K}_\xi = \xi(4\pi/3\sqrt{3}a)\mathbf{e}_x$ , where  $\xi = \pm$  is the valley isospin. Looking for low energy effective theory, we expand the annihilation operators as:

$$a(\mathbf{r}_{mn}) = a_+(\mathbf{r}_{mn})e^{-i\mathbf{K}\cdot\mathbf{r}_{mn}} + a_-(\mathbf{r}_{mn})e^{i\mathbf{K}\cdot\mathbf{r}_{mn}}, \quad (\text{A4})$$

in terms of the slowly-varying fields  $a_\xi(\mathbf{r}_{mn})$  (a similar equation holds for  $b_\xi(\mathbf{r}_{mn})$  operators). Substituting into Eq. A3 and going from lattice to continuum fields as

$$\begin{aligned} \sum_{\mathbf{r}_{mn}} &\rightarrow \int d^2\mathbf{x}/\mathcal{A}_c \text{ and } a_\xi(\mathbf{r}_{mn}) \rightarrow \sqrt{\mathcal{A}_c}a_\xi(\mathbf{x}) \text{ and } b_\xi(\mathbf{r}_{mn}) \\ &\rightarrow \sqrt{\mathcal{A}_c}b_\xi(\mathbf{x}), \end{aligned} \quad (\text{A5})$$

leads to the effective Hamiltonian<sup>24</sup>:

$$H_0 = v_F \int d^2\mathbf{x} \sum_{\xi=\pm} \Psi_\xi^\dagger(\mathbf{x})(\xi p_x^\xi \sigma_x + p_y^\xi \sigma_y) \Psi_\xi(\mathbf{x}), \quad (\text{A6})$$

where  $v_F = 3at/2\hbar$  is the Fermi velocity and  $(p_x, p_y) = (-i\hbar\partial_x, -i\hbar\partial_y)$  are the components of the canonical momentum. The Pauli matrices  $\sigma_x$  and  $\sigma_y$  act on the lattice isospinors  $\Psi_\xi(\mathbf{x}) = (a_\xi(\mathbf{x}), b_\xi(\mathbf{x}))$ .

In the presence of a slowly varying deformation field  $\delta t_i(\mathbf{r}_{mn}) = \delta t_i(\mathbf{x})$ , the valleys remain decoupled and the effective Hamiltonian reads:

$$H_0 = v_F \int d^2\mathbf{x} \sum_{\xi=\pm} \Psi_\xi^\dagger(\mathbf{x})(\xi \Pi_x^\xi \sigma_x + \Pi_y^\xi \sigma_y) \Psi_\xi(\mathbf{x}), \quad (\text{A7})$$

where  $\Pi^\xi = \mathbf{p} + \xi e\mathbf{A}$  shows the coupling of the electronic charge  $-e$  with a valley-dependent gauge field  $\mathbf{A}_\xi(\mathbf{x}) = \xi\mathbf{A}(\mathbf{x})$  defined by:

$$ev_F(A_x(\mathbf{x}) + iA_y(\mathbf{x})) = \sum_{i=1,2,3} \delta t_i(\mathbf{x}) e^{i\mathbf{k}\cdot\boldsymbol{\delta}_i}. \quad (\text{A8})$$

More specifically using Eq. A2, one obtains the gauge vector potential in terms of the deformation field:

$$\begin{aligned} ev_F A_x &= -\frac{1}{2}(\delta t_1 + \delta t_2) + \delta t_3, \\ ev_F A_y &= \frac{\sqrt{3}}{2}(\delta t_1 - \delta t_2), \end{aligned} \quad (\text{A9})$$

where all the position arguments  $\mathbf{x}$  have been omitted.

### 3. Example of a deformation pattern and its induced gauge field

We now consider a particular deformation field where only the bonds along  $\boldsymbol{\delta}_3 = -a\mathbf{e}_y$  are modified according to the pattern

$$(\delta t_1, \delta t_2, \delta t_3) = ev_F B y(0, 0, -1). \quad (\text{A10})$$

According to Eq. 9, the corresponding strain-induced vector potential is the familiar vector potential of the Landau gauge  $\mathbf{A} = -By\mathbf{e}_x$  describing here a uniform magnetic field  $\mathbf{B} = B\mathbf{e}_z$  in the valley  $\xi = +$ , and the opposite field in valley  $\xi = -$ . In this gauge, the natural geometry is a rectangular one with linear sizes  $L_x$  and  $L_y$ . Due to translational invariance, the system can be infinite in the  $x$ -direction but the smooth deformation condition

( $\delta t_3 \ll t$ ) brings a limitation on the transverse size  $L_y$  because  $\delta t_3$  is growing linearly long the  $y$ -direction. Assuming  $\delta t_3(y=0) = 0$ , then  $\delta t_3(L_y) = ev_F B L_y$  cannot exceed a reasonable fraction of  $t = 2\hbar v_F/3a$  which leads to the condition:

$$L_y \ll \frac{\Phi_0}{|B|} \frac{1}{a} = \frac{l_B^2}{a}. \quad (\text{A11})$$

Typically for a magnetic length  $l_B = \sqrt{\hbar/eB} \simeq 10$  nm and lattice constant  $a \simeq 0.1$  nm, the ribbon width cannot exceed 500 nm. The strength of the effective magnetic field  $B$  is proportional to the gradient of the hopping amplitude deformation. For a similar global deformation over the whole sample, a narrow ribbon hosts a stronger magnetic field than a broader ribbon. Note that many other deformation fields lead to the same gauge vector potential, including  $(\delta t_1, \delta t_2, \delta t_3) = ev_F B y(2, 0, 0)$  or  $(\delta t_1, \delta t_2, \delta t_3) = ev_F B y(0, 2, 0)$ .

### 4. Single electron wavefunctions

We derive here the wavefunctions for noninteracting Dirac fermions under a strong pseudo-magnetic field ( $\xi B\mathbf{e}_z$ ), or more precisely the valley-dependent gauge potential  $\mathbf{A}_\xi(\mathbf{x}) = \xi\mathbf{A}(\mathbf{x})$ , which are both opposite fields in the valleys  $\xi = \pm$ . We choose  $B$  positive for definiteness, and denotes  $l_B = \sqrt{\hbar/eB}$  the magnetic length. For each valley, we consider the first quantized Hamiltonian corresponding to Eq. A7, namely:

$$h_\xi = v_F \sum_{\xi} (\xi \Pi_x^\xi \sigma_x + \Pi_y^\xi \sigma_y), \quad (\text{A12})$$

where the components of the gauge-independent momentum  $\Pi^\xi = \mathbf{p} + \xi e\mathbf{A}$  do not commute due to the presence of the pseudo-magnetic field. Unlike the real magnetic field case, the sign of the commutator:

$$[\Pi_x^\xi, \Pi_y^\xi] = -i\xi \frac{\hbar^2}{l_B^2}, \quad (\text{A13})$$

depends on the valley index  $\xi$ . Hence the ladder operators are defined as

$$a_\xi = \frac{l_B}{\sqrt{2}\hbar} (\Pi_x - i\xi \Pi_y), \quad (\text{A14})$$

in order to enforce the proper commutation relation  $[a_\xi, a_\xi^\dagger] = 1$ . The Hamiltonian can be written as:

$$h_\xi = \xi \frac{\hbar v_F \sqrt{2}}{l_B} \begin{pmatrix} 0 & a_\xi \\ a_\xi^\dagger & 0 \end{pmatrix}. \quad (\text{A15})$$

We now focus on the zero energy Landau level. The corresponding wave function in the  $\xi$ -valley is  $(0, v_\xi)$  with  $a_\xi v_\xi = 0$ . Hence in the zero energy level, single electron wavefunctions are finite only on one triangular sublattice, here the B-atoms sublattice (since we have chosen

the field strength  $B$  to be positive). This is a general property valid for any strain-induced gauge field on the graphene lattice.

Now we give explicitly the wavefunctions for the Landau gauge field  $\mathbf{A} = -By\mathbf{e}_x$ . Then the equation  $a_\xi v_\xi = 0$  reads:

$$\left[ (-i\hbar \frac{\partial}{\partial x} - eB\xi y) - \xi\hbar \frac{\partial}{\partial y} \right] v_\xi(x, y) = 0, \quad (\text{A16})$$

and substituting  $v_\xi(x, y) = f_\xi(y)e^{ikx}$  in it, we get

$$\left( \frac{d}{dy} + \frac{y - \xi kl_B^2}{l_B^2} \right) f_\xi(y) = 0. \quad (\text{A17})$$

Finally the normalized wavefunction is:

$$v_\xi(x, y) = \frac{1}{\sqrt{\pi^{1/2} L_x l_B}} e^{-\frac{1}{2l_B^2}(y - \xi kl_B^2)^2} e^{ikx}. \quad (\text{A18})$$

Those wavefunctions correspond to the continuum model. For the numerical calculations on the honeycomb lattice (performed to obtain the results in Figs. 2,3,4 of the main text), the wavefunctions are different from Eq. A18 and have to be determined numerically using lattice model with pseudo magnetic field. Nevertheless for the  $n = 0$ -Landau level, there is a simple procedure to get the wavefunctions in the pseudo gauge field  $\xi\mathbf{A}$  from the ones in the usual valley-independent gauge field  $\mathbf{A}$ . As said before for the real magnetic field, the ( $\xi = +$ )-valley wavefunctions have predominant weight on B atoms, and ( $\xi = -$ )-valley wavefunctions on A atoms. To get the corresponding wavefunctions in a pseudo magnetic field, one has simply to i) keep the former ( $\xi = +$ )-valley wavefunctions on B atoms without any change, and ii) swap the later ( $\xi = -$ )-valley wavefunctions from A to B atoms while taking the complex conjugate of those wavefunctions in the meantime.

## 5. Effect of interactions

Here we will consider the projection of density-density interactions of the form  $H_I = \sum_{\mathbf{r}, \mathbf{r}'} V(\mathbf{r} - \mathbf{r}') n(\mathbf{r}) n(\mathbf{r}')$  into the  $n = 0$  PLL which then would have the form:

$$H_I^{n=0} = \sum_{P_1, P_2, P_3, P_4, \sigma, \sigma'} V_{P_1, P_2, P_3, P_4} c_{\sigma, P_1}^\dagger c_{\sigma', P_2}^\dagger c_{\sigma, P_3} c_{\sigma', P_4}, \quad (\text{A19})$$

where  $c_{P, \sigma}^\dagger$  is the creation operator of fermion in state  $P = \{\xi, k\}$  which is in valley  $\xi$  and Landau orbital  $k$  (see eqn. A18).

Using the continuum model derived in the last section we get the the projected potential:

$$V_{P_1, P_2, P_3, P_4} = \left( \frac{g^2 a^2}{L_x l} \right)^2 \int d\mathbf{r} d\mathbf{r}' V(\mathbf{r} - \mathbf{r}') (-i)^{\xi_3 + \xi_4 - \xi_1 - \xi_2} e^{-\frac{1}{4l^2} [(k_1 l^2 - y)^2 + (k_2 l^2 - y')^2 + (k_3 l^2 - y)^2 + (k_4 l^2 - y)^2]} e^{i\frac{4\pi}{3a} [(\xi_1 - \xi_4)x + (\xi_2 - \xi_3)x']} e^{-i[(k_1 \xi_1 - k_4 \xi_4)x + (k_2 \xi_2 - k_3 \xi_3)x']}, \quad (\text{A20})$$

where  $g = \left( \frac{3}{84\pi} \right)^{\frac{1}{4}}$ . We can now consider different interaction potentials.

If the interaction is smooth the dominant interaction term has  $\xi_1 = \xi_4$  and  $\xi_2 = \xi_3$ .

There are two polarized states which will be particularly of our interest. valley  $|\psi_V\rangle = \Pi_k c_{1, k, \uparrow}^\dagger c_{1, k, \downarrow}^\dagger$  or spin  $|\psi_S\rangle = \Pi_k c_{1, k, \uparrow}^\dagger c_{-1, k, \uparrow}^\dagger$  polarized states. The energy of these states have the general form of:

$$E_V = \sum_{\{p_1, 1\}, \{p_2, 1\}, \sigma, \sigma'} V_{\{p_1, 1\}, \{p_2, 1\}, \{p_2, 1\}, \{p_1, 1\}} - V_{\{p_1, 1\}, \{p_2, 1\}, \{p_1, 1\}, \{p_2, 1\}} \delta_{\sigma, \sigma'}, \quad (\text{A21})$$

and

$$E_S = \sum_{\{p_1, \xi_1\}, \{p_2, \xi_2\}} V_{\{p_1, \xi_1\}, \{p_2, \xi_2\}, \{p_2, \xi_2\}, \{p_1, \xi_1\}} - V_{\{p_1, \xi_1\}, \{p_2, \xi_2\}, \{p_1, \xi_1\}, \{p_2, \xi_2\}} \delta_{\xi_1, \xi_2}. \quad (\text{A22})$$

## 6. Coulomb interaction

Putting the Coulomb interaction  $V(\mathbf{r}_i - \mathbf{r}_j) n(\mathbf{r}_i) n(\mathbf{r}_j) = e^2 n(\mathbf{r}_i) n(\mathbf{r}_j) / 4\pi \epsilon |\mathbf{r}_i - \mathbf{r}_j|$  in projection A20:

$$V_{P_1, P_2, P_3, P_4} = \left( \frac{g^2 a^2}{L_x l} \right)^2 \int d\mathbf{r} d\mathbf{r}' \frac{q^2}{|\mathbf{r} - \mathbf{r}'|} e^{-\frac{1}{24l^2} [(k_1 l^2 - y)^2 + (k_2 l^2 - y')^2 + (k_3 l^2 - y)^2 + (k_4 l^2 - y)^2]} e^{-i[\xi_1(k_1 - k_4)x + \xi_2(k_2 - k_3)x']} \quad (\text{A23})$$

For neutral graphene the  $n = 0$  PLL is at half filling. The interactions naturally prefers the polarized state of valley or spin degrees of freedom. Using A22 the energy of spin polarized state is given by:

$$E_S = \sum_{p_1, p_2} \left( \frac{g^2 a^2}{L_x l} \right)^2 L_x \int d(x - x') dy dy' \frac{q^2}{\sqrt{(x - x')^2 + (y - y')^2}} 2 \left( 2e^{-\frac{1}{2l^2} [(p_1 l^2 - y)^2 + (p_2 l^2 - y')^2]} - \cos[(p_1 - p_2)(x - x')] e^{-\frac{1}{4l^2} [(p_1 l^2 - y)^2 + (p_1 l^2 - y')^2 + (p_2 l^2 - y)^2 + (p_2 l^2 - y')^2]} \right) \quad (\text{A24})$$



Interestingly the valley polarized state has the same energy:  $E_V = E_S$ . If we include the fast oscillation which we ignored before ( $e^{i\frac{4\pi}{3a}[(\xi_1 - \xi_4)x + (\xi_2 - \xi_3)x']}$ ), the valley polarized state does not change since  $\xi_1 = \xi_2 = \xi_3 = \xi_4$ , but the energy of spin polarized state increases, so the valley polarized state will be the ground state of neutral graphene if the long range Coulomb is the dominating interaction.

Notice that we considered a valley polarized state in a single valley. If we consider an arbitrary rotated valley polarized state in a state of the form:

$$|\psi_{V'}\rangle = \Pi(u_k^+ c_{+,k,\uparrow}^\dagger + u_k^- c_{-,k,\uparrow}^\dagger, k, \uparrow)(u_k^+ c_{+,k,\downarrow}^\dagger + u_k^- c_{-,k,\downarrow}^\dagger)|0\rangle, \quad (\text{A25})$$

the Hartree-Fock energy have the form:

$$E_{V'} = E_V + 2 \sum_{p_1 \neq p_2} \Gamma_{p_1, p_2} \sum_{\xi} |u_{p_1}^{-\xi}|^2 |u_{p_2}^{\xi}|^2, \quad (\text{A26})$$

where  $\Gamma_{p_1, p_2}$  is positive for the Coulomb potential. The term added is then always positive and the minimum of energy is for  $u_p^+ = 0$  or  $u_p^- = 0$  for all  $p$ . The preferred state would be an Ising valley polarized state.

## 7. Short rang Hubbard interactions and superconductivity

Although all types of density-density interactions could be treated using our projection scheme, here we only present the details for the on-site and next nearest neighbor interactions which we also studied numerically and observed the somehow unexpected spin polarized superconductivity.

The on-site interaction has the form  $\int d\mathbf{r}d\mathbf{r}' V \delta(\mathbf{r} - \mathbf{r}')$  where as next-nearest neighbor interaction has the form  $\int d\mathbf{r}d\mathbf{r}' V \sum_{i=1}^6 \delta(\mathbf{r} + \mathbf{R}_i - \mathbf{r}')$  where  $\mathbf{R}_i = (X_i, Y_i)$  are the vectors connecting each site to its six next nearest neighbors. This next nearest neighbour interaction projected into the  $n = 0$  PLL has the form:

$$V_{P_1, P_2, P_3, P_4} = V \left( \frac{g^2 a^2}{L_x l} \right)^2 L_x \int dy e^{-\frac{1}{l^2} \left[ (y - \frac{p_1 + p_2 + p_3 + p_4}{4} l^2)^2 + l^4 \frac{\sum (p_i - p_j)^2}{32} \right]} \Omega(\xi_2 - \xi_3). \quad (\text{A27})$$

Here we have  $\xi_2 - \xi_3 = \xi_4 - \xi_1$  and  $\xi_1 p_1 + \xi_2 p_2 - \xi_3 p_3 - \xi_4 p_4 = 0$ . Notice that the interaction is not smooth in the lattice scale so we should keep the oscillatory term  $\Omega(\xi_2 - \xi_3) = \sum_{i=1}^6 e^{i\frac{4\pi}{3a}(\xi_2 - \xi_3)X_i} = 2 \cos \left[ \frac{4\pi}{3}(\xi_2 - \xi_3) \right] + 4 \cos \left[ \frac{2\pi}{3}(\xi_2 - \xi_3) \right]$ .

For on-site interaction we have similar form with  $\Omega(\xi_2 - \xi_3) = 1$ .

With this form of the projected interaction potential we can readily compare the energy of spin and valley

polarized states. Using the expressions in A21 and A22 we get:

$$E_V = V \frac{g^4 a^4}{L_x l^2} \int dy \sum_{p_1, p_2} e^{-\frac{1}{l^2} \left[ (y - \frac{p_1 + p_2}{2} l^2)^2 + l^4 \frac{(p_1 - p_2)^2}{16} \right]} \sum_{\sigma, \sigma'} \Omega(0) (1 - \delta_{\sigma, \sigma'}), \quad (\text{A28})$$

and

$$E_S = V \frac{g^4 a^4}{L_x l^2} \int dy \sum_{p_1, p_2} e^{-\frac{1}{l^2} \left[ (y - \frac{p_1 + p_2}{2} l^2)^2 + l^4 \frac{(p_1 - p_2)^2}{16} \right]} \sum_{\xi_1, \xi_2} \Omega(0) - \Omega(\xi_2 - \xi_1). \quad (\text{A29})$$

For the on-site interaction with  $\Omega(\xi_2 - \xi_1) = 1$  the spin polarized state has no energy-gain where as valley polarized state energy increases with on site repulsion.

For the next nearest neighbour interaction  $\Omega(\xi_2 - \xi_1) = \Omega(0) \left( \frac{3}{2} \delta_{\xi_1, \xi_2} - 1 \right) < \delta_{\xi_1, \xi_2}$ . So valley polarized state will be stabilized with next nearest neighbor interactions.

With the projected interaction of the general form  $\sum_{P_1, P_2, P_3, P_4, \sigma, \sigma'} V_{P_1, P_2, P_3, P_4} c_{\sigma, P_1}^\dagger c_{\sigma', P_2}^\dagger c_{\sigma, P_3} c_{\sigma', P_4}$  we can also compare the mean-field energy of different superconducting states. We compare the energy of two superconducting states which are valley triplet, spin singlet:

$$|\Psi_{Singlet}\rangle = \Pi_{P_i = \{+, p_i\}, \{-, p_i\}} (u_i + v_i c_{P_i, \uparrow}^\dagger c_{P_i, \downarrow}^\dagger) |0\rangle, \quad (\text{A30})$$

and spin triplet, valley singlet:

$$|\Psi_{Triplet}\rangle = \Pi_{P_i = \{+, p_i\}, \sigma = \uparrow, \downarrow} (u_i + v_i c_{P_i, \sigma}^\dagger c_{\bar{P}_i, \bar{\sigma}}^\dagger) |0\rangle, \quad (\text{A31})$$

where  $\bar{P}$  and  $\bar{\sigma}$  are the time reversal of  $P$  and  $\sigma$  respectively.

The corresponding mean-field equations for the superconducting gap for the spin singlet state reads:

$$\Delta_P = - \sum_{P' = \{+, p_i\}, \{-, p_i\}} V_{P, \bar{P}, \bar{P}', P'} u_{P'} v_{P'}, \quad (\text{A32})$$

and for the spin triplet state reads:

$$\Delta_P = - \sum_{P' = \{+, p_i\}, \sigma = \uparrow, \downarrow} V_{P, \bar{P}, \bar{P}', P'} u_{P'} v_{P'}, \quad (\text{A33})$$

where

$$V_{P, \bar{P}, \bar{P}', P'} = V \left( \frac{g^2 a^2}{L_x l} \right)^2 L_x \int dy e^{-\frac{1}{l^2} \left[ (y - \frac{p + p'}{2} l^2)^2 + l^4 \frac{\sum (p - p')^2}{16} \right]} \left( 2 \cos \left[ \frac{4\pi}{3}(\xi_2 - \xi_3) \right] + 4 \cos \left[ \frac{2\pi}{3}(\xi_2 - \xi_3) \right] \right)$$

In the spin-singlet state  $V_{P,\bar{P},\bar{P}',P'}$  changes sign between the states with  $\xi' = -\xi$  and  $\xi' = \xi$ , where as for the spin triplet for all the term in the mean field equation have  $\xi' = \xi$ . So we get larger gap and so smaller mean-field energy for the spin triplet superconducting state.

### 8. The robustness of the fractional valley Hall insulator and its evolution with tuning $U_{nnn}^s$

The fractional valley Hall insulator is characterized by a large ground state degeneracy. In a finite-size system, due to the coupling between different states, one usually sees a quasi-degeneracy with a finite splitting between these states in the ground state manifold. As shown in Fig. 4, around  $U_{nnn}^{op} = -0.6$  without the interaction between the electrons in the same valley  $U_{nnn}^s = 0$ , the nine states at the right quantum number sectors are indeed have much lower energy than other excited states. However, the splitting between these states are close to the finite gap between these states and other excited states. While the quantized nonzero total Chern number of the ground state manifold indicates the obtained state is indeed a fractional valley Hall insulator, a clear-cut evidence of nine fold topological degeneracy is still absent and it is difficult to predict the fate of the state as system becomes very large. Here we address this issue through tuning the system deep into the topological phase. Indeed this can be achieved by increasing the correlations between the electrons in the same valley ( $U_{nnn}^s$ ).

As shown in Fig. 5, with the turn on of positive  $U_{nnn}^s$ , the energy gap between the ground state manifold and other excited states becomes very robust and much larger than the splitting of the energy of the ground state manifold. There is no phase transition as  $U_{nnn}$  continuously increases, so the observed state is indeed the same phase as the fractional valley Hall insulator at the decoupled limit (strong  $U_{nnn}^s$  limit). In that limit, the nine fold degeneracy is exact and spinless electrons in different valleys are contributing  $\pm 1/3$  quantized Hall conductances. We further perform the flux inserting measurement. we show in Fig. 5b for  $U_{nnn}^s = 1$ , the three lowest energy states in the momentum sector  $k = 0$  evolve into other states in the ground state manifold and they evolve back to themselves after three periods of boundary phase insertion. The energy gap between these states and other excited states remain robust as illustrated in Fig. 5b. We further perform valley-dependent Chern number calculation<sup>36,37</sup>, and find a total Chern number quantized to 6 for all nine levels, characterizing the  $2/3$  fractionalized valley spin-Hall effect<sup>37</sup>. Remarkably, this phase persists in a wide range of  $U_{nnn}^s \geq -0.2$  including the simple case where this interaction is turned off

( $U_{nnn}^s = 0$  as shown in the main text part of the paper.

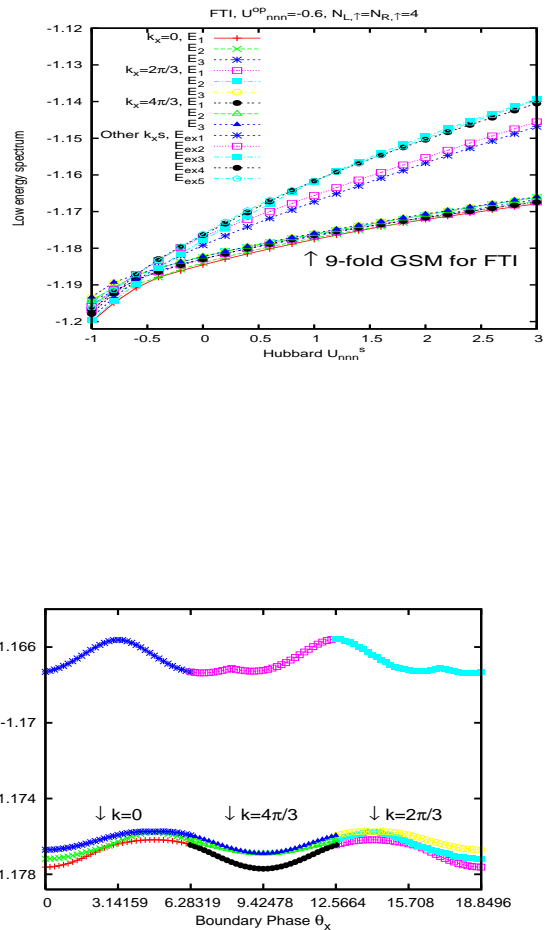


FIG. 5: (Color online) (a) Fractional topological insulating phase for spinless electrons at filling  $\nu = -2 + 2/3$ . The LL degeneracy is  $N_s = 12$  while there are totally  $N_e = 8$  ( $N_L = N_R = 4$ ) electrons with polarized spin on a lattice with  $24 * 24$  sites. We demonstrate an emergent symmetry where energies of nine states from  $k = 0, 2\pi/3$  and  $4\pi/3$  sectors become near degeneracy at large  $U_{nnn}^s$  limit. The onset of the fractionalized phase with nine-fold near degenerating GSM is identified at  $U_{nnn}^s \geq -0.2$ . (b) The evolution and the robust of the gap during the change of the boundary phase.

<sup>1</sup> E. Tang, J.-W. Mei, and X.-G. Wen, Phys. Rev. Lett. **106**, 236802 (2011).

<sup>2</sup> K. Sun, Z. Gu, H. Katsura, and S. Das Sarma, Phys. Rev.

- Lett. **106**, 236803 (2011).
- <sup>3</sup> T. Neupert, L. Santos, C. Chamon, and C. Mudry, Phys. Rev. Lett. **106**, 236804 (2011).
  - <sup>4</sup> D. N. Sheng, Z.-C. Gu, K. Sun, and L. Sheng, Nat. Commun. **10**, 1380 (2011).
  - <sup>5</sup> Y.-F. Wang, Z.-C. Gu, C.-D. Gong, and D. N. Sheng, Phys. Rev. Lett. **107**, 146803 (2011).
  - <sup>6</sup> J. W. Mei, E. Tang, and X. G. Wen, arXiv:1102.2496.
  - <sup>7</sup> N. Regnault and B. A. Bernevig, arXiv:1105.4867.
  - <sup>8</sup> X.-L. Qi, Phys. Rev. Lett. **107**, 126803 (2011).
  - <sup>9</sup> M. Levin and A. Stern, Phys. Rev. Lett. **103**, 196803 (2009).
  - <sup>10</sup> J. Maciejko, X.-L. Qi, A. Karch, and S.-C. Zhang, Phys. Rev. Lett. **105**, 246809 (2010).
  - <sup>11</sup> T. Neupert, L. Santos, S. Ryu, C. Chamon, and C. Mudry, Phys. Rev. B **84**, 165107 (2011).
  - <sup>12</sup> L. Levy and al., Science **329**, 544 (2010).
  - <sup>13</sup> F. Guinea, M. I. Katsnelson, and A. K. Geim, Nat. Phys. **6**, 30 (2010).
  - <sup>14</sup> T. Low and F. Guinea, Nano Lett. **10**, 3551 (2010).
  - <sup>15</sup> A. Singha, M. Gibertini, B. Karmakar, S. Yuan, M. Polini, G. Vignale, M. I. Katsnelson, A. Pinczuk, L. N. Pfeiffer, K. W. West, et al., Science **332**, 1176 (2011).
  - <sup>16</sup> P. Soltan-Panahi and *et al.*, Nature Physics **7**, 434 (2011).
  - <sup>17</sup> A. H. C. Neto, F. Guinea, N. M. R. Peres, K. S. Novoselov, and A. K. Geim, Rev. Mod. Phys. **81**, 109 (2009).
  - <sup>18</sup> B. Uchoa and A. Castro Neto, Phys. Rev. Lett. **98**, 146801 (2007).
  - <sup>19</sup> N. Kopnin, T. Heikkila, and G. Volovik, Phys. Rev. B **83**, 220503 (2011).
  - <sup>20</sup> M. Kiesel, C. Platt, W. Hanke, D. Abanin, and R. Thomale, arXiv:1109.2953.
  - <sup>21</sup> J. Alicea and M. Fisher, Phys. Rev. B **74**, 075422 (2006).
  - <sup>22</sup> M. Goerbig, R. Moessner, and B. Doucot, Phys. Rev. B **74**, 161407 (2006).
  - <sup>23</sup> L. Sheng, D. Sheng, F. D. M. Haldane, and L. Balents, Phys. Rev. Lett. **99**, 196802 (2007).
  - <sup>24</sup> M. Goerbig, Rev. Mod. Phys. **83**, 1193 (2011).
  - <sup>25</sup> Y. Barlas, K. Yang, and A. H. MacDonald, arXiv:1110.1069.
  - <sup>26</sup> F. Guinea, M. I. Katsnelson, and K. S. Novoselov, Phys. Rev. B **77**, 075422 (2010).
  - <sup>27</sup> T. O. Wehling, E. Sasioglu, C. Friedrich, A. Lichtenstein, M. Katsnelson, and S. Blugel, Phys. Rev. Lett. **106**, 236805 (2011).
  - <sup>28</sup> K. I. Bolotin, F. Ghahari, M. D. Shulman, H. L. Stormer, and P. Kim, Nature **462**, 196 (2009).
  - <sup>29</sup> X. Du, I. Skachko, F. Duerr, A. Luican, and E. Y. Andrei, Nature **462**, 192 (2009).
  - <sup>30</sup> C. R. Dean, A. F. Young, P. Cadden-Zimansky, L. Wang, H. Ren, K. Watanabe, T. Taniguchi, P. Kim, J. Hone, and K. L. Shepard, Nat. Phys. **7**, 693 (2011).
  - <sup>31</sup> C. Toke and J. Jain, Phys. Rev. B **75**, 245440 (2007).
  - <sup>32</sup> M. Goerbig and N. Regnault, Phys. Rev. B **75**, 241405 (2007).
  - <sup>33</sup> I. McDonald and F. Haldane, Phys. Rev. B **53**, 15845 (1996).
  - <sup>34</sup> D. Thouless, M. Kohmoto, M. and Nightingale, and M. den Nijs, Phys. Rev. Lett. **49**, 405 (1982).
  - <sup>35</sup> Q. Niu, D. J. Thouless, and Y.-S. Wu, Phys. Rev. B **31**, 3372 (1985).
  - <sup>36</sup> D. N. Sheng and L. Balents, Phys. Rev. Lett. **91**, 116802 (2003).
  - <sup>37</sup> D. N. Sheng, Z. Y. Weng, L. Sheng, and F. D. M. Haldane, Phys. Rev. Lett. **97**, 036808 (2006).
  - <sup>38</sup> R. G. Melko, A. Paramakanti, A. A. Burkov, A. Vishwanath, D. N. Sheng, and L. Balents, Phys. Rev. Lett. **95**, 127207 (2005).
  - <sup>39</sup> Z. Papic, R. Thomale, and D. A. Abanin, Phys. Rev. Lett. **107**, 176602 (2011).
  - <sup>40</sup> C. H. Park and S. Louie, Nano Lett. **9**, 1793 (2009).